IEEE Access
Multidisciplinary ⋮ Rapid Review ⋮ Open Access Journal

Received July 23, 2020, accepted August 14, 2020, date of publication August 19, 2020, date of current version August 31, 2020.

Digital Object Identifier 10.1109/ACCESS.2020.3018027

Passivity-Based Control for Small Hydro-Power Generation With PMSG and VSC

WALTER GIL-GONZÁLEZ[1], (Member, IEEE), ALEJANDRO GARCÉS[2], (Senior Member, IEEE), AND OLAV B. FOSSO[3], (Senior Member, IEEE)

[1]Grupo GIIEN, Facultad de Ingeniería, Institución Universitaria Pascual Bravo, Medellín 050036, Colombia
[2]Department of Electric Power Engineering, Universidad Tecnológica de Pereira, Pereira 660003, Colombia
[3]Department of Electric Power Engineering, Norwegian University of Science and Technology, 7491 Trondheim, Norway

Corresponding author: Walter Gil-González (wjgil@utp.edu.co)

This work was supported in part by the Administrative Department of Science, Technology, and Innovation (COLCIENCIAS) of Colombia through the National Scholarship Program under Grant 727-2015.

ABSTRACT This paper presents a passivity-based control method for a small hydro-power system that consists of a permanent magnet synchronous generator (PSMG) connected to the grid through a back-to-back converter. Nonlinear models of the hydraulic, mechanical, and electrical parts of the small hydro-power system are considered. Two approaches in the realm of passivity-based control are implemented, namely, standard passivity-based control and PI-passive. These controls consider the intrinsic characteristics of the model, which has a port-Hamiltonian (pH) structure with a small hydro-power system in open-loop. The purpose is to design a control law with passive output which ensures asymptotic stability for closed-loop operation in the sense of Lyapunov's theory. The paper is practically oriented, and hence, the proposed controllers are tested and compared with a conventional approach, in a 13.2 kV distribution feeder. The proposed controllers have been assessed and compared with a classical PI controller considering steady state and transient behaviors in small hydro-power plants (SHPs). Simulation results show that the proposed methodology guarantees stability and offers better dynamical performance.

INDEX TERMS Small hydro-power, permanent magnet synchronous generation (PMSG), energy conversion power systems, passivity, back-to-back converter.

I. INTRODUCTION

Small hydro-power plants (SHPs) are well known renewable energy sources with foreseeable energy production, at least in the short term, compared to other types of renewable energy sources such as photovoltaic and wind power. An SHP is usually composed of a reservoir, water tunnel, penstock, hydraulic turbine, speed governor, and generator. Modern systems may include a power electronic converter, as shown in Fig. 1, which allows high efficiency due to the opportunity of variable speed operation. This system has a strong coupling between mechanical, hydraulic, and electrical dynamics which makes the system difficult to analyze [1], [2]. Moreover, it presents many different operating points, which also complicate the analysis [3]. These features make the design and control of this system challenging.

Several works have focused on proposing controllers for governor systems. Typically, two types of governor controller can be found in the literature, namely, which are proportional-integral-derivative (PID) [4]–[6] and state feedback controller [7]–[10]. PID controllers' design is based on system outputs and does not use the internal information of the SHP. Therefore, it is challenging to guarantee the stability for all operating points since linear models oversimplify the system dynamics. In the case of state feedback controllers, several controllers have been proposed such as nonlinear control [9], [10], intelligent control [8], sliding mode control [2], [11], fuzzy control [12]–[14], fault-tolerant control [15], predictive control [7], [16], synergetic control [17] and finite-time control [18]. However, these controls are observed to be difficult to implement and require tuning of many parameters and perform an on-line optimization process [18]. Most of these investigations analyze only one part of the system, for example, the hydraulic and/or mechanical dynamics without taking into account the electrical part.

The associate editor coordinating the review of this manuscript and approving it for publication was Fengjiang Wu.

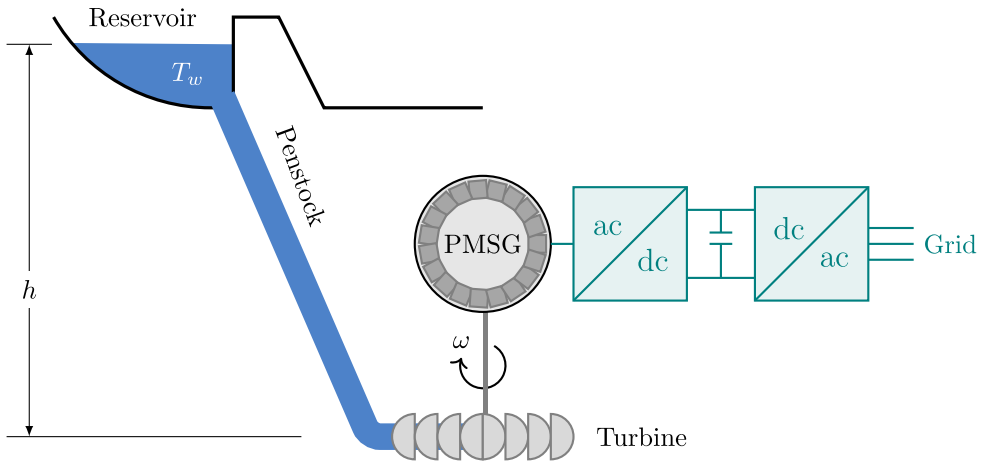

FIGURE 1. Proposed small hydro-power system with PMSG and back-to-back converter with hydraulic, mechanical and electrical subsystems.

Recent investigations have demonstrated the advantages of including power electronic devices into the energy conversion system to improve efficiency by allowing variable speed [3]. In [19] and [20], a model SHP connected to the ac grid using a permanent magnet synchronous generator (PMSG), diode bridge rectifier, boost converter and voltage source converter (VSC) was studied. This configuration was also used in wind power applications in [21], [22]. The model proposed in [20] was improved in [3] and presented a detailed analysis where high efficiency was achieved by reducing the electrical power losses. In [23], a multilevel hierarchical structure based on a PI controller was proposed; however, in that work, hydraulic dynamics were not considered.

Unlike these previous works, we take advantage of the port-Hamiltonian (pH) structure that presents the SHP in open-loop for the purpose of designing a controller based on passivity theory that keeps its pH structure in closed-loop and guarantees asymptotic stability in the sense of Lyapunov. The main contributions of the paper are summarized below:

- Presents a mathematical model for an SHP employing a PMSG which is connected to the grid through a back-to-back converter. This model contains hydraulic, mechanical, and electrical (PMSG and VSC) dynamics, all of which are shown as a pH structure.
- Designs a controller based on the passivity theory for SHP. Passivity-based control (PBC) is employed since the mathematical model for SHP in an open-loop exhibits a passive structure, making it suitable to apply the passivity theory. The proposed control considers the complete nonlinear model of the system and guarantees local asymptotic stability in the sense that Lyapunov maintains its passive structure.
- Makes an analysis of the performance of the proposed controller under conditions of stable transient responses to demonstrate its robustness.
- Compares the PBC with a conventional PI controller, where the proposed controller presents better performance in all cases considered.

The remainder of all the paper is organized as follows: In Section II, the dynamic model of the SHP and its pH representation are presented. Next, in Section III, the passivity-based control and controller design for the SHP are described. Following this, simulation results and main comments are presented. Finally, some conclusions are drawn in Section V.

II. SMALL HYDRO-POWER PLANT

The hydraulic and mechanical parts consist of a hydro-turbine, a governor system, and a penstock. The governor's main function is to control the speed and power output by adjusting the hydraulic turbine's water flow. Typical governor systems consist of PID controls [10], [24]. The electrical part is composed of a PMSG connected to the grid through a back-to-back converter. Both parts exhibit a passivity structure which is used to design the control.

A. HYDRAULIC TURBINE

The model considers an incompressible fluid as recommended by the IEEE working group on prime movers and energy supply models [26]. This model considers the dynamics of the penstock, the tunnel and the turbine as well as the head losses (see Fig. 1), as follows:

$$T_w \dot{q} = 1 - h - k_f q^2, \tag{1}$$

where h is the hydraulic head, k_f defines the friction losses on the conduit; q is the normalized flow on the penstock and T_w is the starting time of water on the penstock, which is defined as

$$T_w = \frac{L q_{base}}{A h_{base} g}, \tag{2}$$

where q_{base} is flow rate when the gates are fully open, h_{base} defined as the static head of the water column above the turbine [10]; L and A are the length and the area of the penstock, and g denotes the acceleration of gravity.

The hydraulic head and the mechanical power of the turbine in per-unit values are given by

$$\begin{aligned} h &= \left(\frac{q}{y}\right)^2, \\ P_m &= A_t h \left(q - q_{nl}\right), \end{aligned} \tag{3}$$

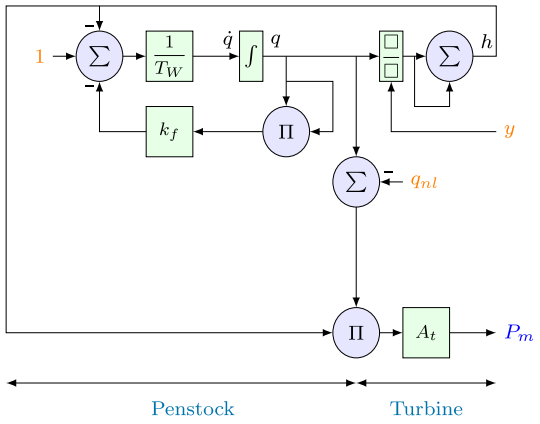

FIGURE 2. Nonlinear model of hydraulic turbine.

where y represents the gate position, A_t is a proportional constant and q_{nl} is the no-load flow rate of the hydro-turbine. Fig. 2 illustrates the nonlinear turbine model described from (1) to (3). The hydraulic servo model can be described by

$$T_y\dot{y} = u_y - y, \tag{4}$$

where T_y is the time constant of the servomotor and u_g denotes input control, which is generally built with PID controls.

B. PERMANENT MAGNET SYNCHRONOUS GENERATOR

Fig. 1 shows a PMSG connected to the power grid with a back-to-back converter [25], [27]. The electrical and mechanical equations that describe the behavior of the dynamics in values per-unit of a PMSG are given by

$$\begin{aligned} L_g\dot{i}_{dg} &= -R_g i_{dg} + L_g\omega_m i_{qg} - v_d, \\ L_g\dot{i}_{qg} &= -R_g i_{qg} - L_g\omega_m i_{dg} + \psi\omega_{e_g} - v_q, \\ M\dot{\omega}_m &= T_m - T_e, \end{aligned} \tag{5}$$

with

$$M = \frac{2H_g}{\omega_o}, \tag{6}$$

where v_d, v_q, i_{dg} and i_{qg} are the voltages and currents of PMSG in dq reference frame, respectively. R_g and L_g are the stator winding's resistance and inductance, respectively. ω_m is the rotor speed ($\omega_m = \omega_{e_g}$ in per–unit). ψ denotes permanent magnetic flux produced by the rotor magnets, which is constant and depends on the material used for its construction. H_g is hydro–turbine inertia time constant and ω_o is the generator based angular speed; T_m and T_e are the mechanical and electrical torque. Mechanical torque T_m is obtained readily from (3) as

$$T_m = \frac{P_m}{\omega_m} = \frac{A_t q^2\,(q - q_{nl})}{y^2\omega_m}, \tag{7}$$

and the electrical torque is given by

$$T_e = \psi i_q. \tag{8}$$

Typically a back-to-back configuration with voltage source converters is employed to integrate a PMSG to the ac grid since this requires a full-rated converter [27]. Therefore, the output voltages of a PMSG can be defined as a function of the modulation indices of the converter as follows:

$$v_{dq} = m_{dq_g} v_{dc} \tag{9}$$

where $m_{dq_g} \in [-1, 1]$ represents the modulation index and subscript g refers to the VSC_g; v_{dc} is the voltage in the dc-link. The PMSG output voltages are represented as modulation indexes by the voltage in the dc-link (for more details, see [28]).

The dynamical modeling of the second VSC in the dq reference frame is given by

$$\begin{aligned} L\dot{i}_d &= -Ri_d - L\omega_e i_q + v_{dc}m_{d2} - e_d, \\ L\dot{i}_q &= -Ri_q + L\omega_e i_d + v_{dc}m_{q2} - e_q, \\ C\dot{v}_{dc} &= i_s - i_d m_d - i_q m_q, \end{aligned} \tag{10}$$

where i_{dq} are the currents that flow through of the transformer and L and R are their inductance and resistance parameters, respectively. e_{dq} is the ac voltage of the main grid; C is the dc-link capacitor of the VSC and its voltage is v_{dc} and i_s is the current delivered by the PMSG. ω_e is the grid angular electrical frequency, which is found by employing a classical phase-locked loop (PLL) [29]. $m_{dq} \in [-1, 1]$ represents the modulation index of a VSC connected to the ac grid.

C. COMPLETE DYNAMICAL MODEL

The dynamical systems described from (1) to (5) are rewritten in a pH structure,[1] as follows

$$D_g\dot{x}_g = \big(J(x) - R_g(x)\big)\,x_g + b(x) + Gu_g, \tag{11}$$

where $J(x)_{34} = L_g\omega_m$, $J(x)_{45} = \psi$, while

$$x_g = \text{col}(x_1, \ldots, x_5) := \text{col}(q, y, i_{dg}, i_{qg}, \omega_m), \tag{12}$$

$$u_g = \text{col}(u_y, m_{dg}, m_{qg}), \tag{13}$$

$$b(x) = \text{col}(1, 0, 0, 0, T_m), \tag{14}$$

$$D_g = \text{diag}\{T_w, T_y, L_g, L_g, M\} \tag{15}$$

$$R_g(x) = \text{diag}\left\{\left(\frac{1}{x_2^2} + k_f\right)x_1, 1, R_g, R_g, 0\right\} \tag{16}$$

$$G = \begin{bmatrix} 0 & 0 & 0 \\ 1 & 0 & 0 \\ 0 & v_{dc} & 0 \\ 0 & 0 & v_{dc} \\ 0 & 0 & 0 \end{bmatrix}, \tag{17}$$

and dynamical systems (10) can also be written as a pH structure as follows:

$$D_v\dot{x}_v = \left(J_o + \sum_{i=1}^{2} J_i u_{2i} - R_v\right)x_v + d_v, \tag{18}$$

where $J_{o_{13}} = L\omega_e$, $J_{1_{13}} = 1$, $J_{2_{23}} = 1$, while

$$x_v = \text{col}(x_6, x_7, x_8) := \text{col}(i_d, i_q, v_{dc}), \tag{19}$$

$$d = \text{col}(-e_d, -e_q, i_s), \tag{20}$$

$$u_v = \text{col}(m_{d2}, m_{q2}), \tag{21}$$

$$D_v = \text{diag}\{L, L, C\} \tag{22}$$

$$R_v = \text{diag}\{R, R, 0\}, \tag{23}$$

[1] See [30] for further details on pH systems in control applications.

where x_g, x_v, d_g, d_v and u_g, u_v are state, external input and control signal vectors, respectively; D_g, D_v, $R_g(x), R_v$ and J are the generalized inertia, damping and interconnection matrices, respectively.

The term $J_{i_{km}}$ denotes position km of matrix J_i and fulfills that $J_{i_{km}} = -J_{i_{mk}}$. Observe that the matrices defined above satisfy that

$$D_g > 0, \quad D_v > 0,\ R_g \geq 0,\ R_v \geq 0,\ J = -J^\top. \quad (24)$$

In order to design the control, we assume that:

Assumption 1: The water flow rate in normal operation and in per-unit is limited between $q_{nl} < x_1 \leq 1$ (see [31] for a more physical justification of this assumption).

Assumption 2: The gate position in per-unit is limited between $0 < x_2 \leq 1$ (see also [31]).

Assumption 3: Mechanical speed of PMSG is always greater than zero $x_5 > 0$ and the reference mechanical speed of PMSG $\omega_m^{ref} = 1$.

Assumption 4: The dc-link voltage is always greater than zero $v_{dc} > 0$.

Assumption 5: The states and external inputs are measurable and all parameters of the system are known.

Assumptions 1 and 2 are necessary for a machine that delivers active power. The water flow rate is the conduit, and the turbine always moves in the same direction. Assumptions 3 is logical since the rotor speed should always be close to constant. Assumption 4 is necessary for a VSC to operate properly. Assumption 5 is reasonable since measuring rate flow, rotor speed, and currents are standard practice in an SHP.

III. PASSIVITY-BASED CONTROL

The PBC theory is a well-founded technique that has proven to be very useful and powerful in designing robust controllers when applied to dynamical systems with a pH structure [32]. The PBC preserves the pH structure and guarantees stability in closed-loop in the sense of Lyapunov [32], [33]. The standard PBC (S-PBC), IDA-PBC, and PI passive techniques have been widely used in a number of applications, including mechanical, electro-mechanical, and power electronic systems [34]. In this section, the controller designs for SHP and VSC are shown.

A. S-PBC

Given that the system (11) is an input-affine system, it is appropriate to use an S-PBC.[2] Therefore, the system (11) can be described in closed-loop as follows

$$D_g \dot{e}_g = \big(J(x) - R_g(x)\big)\, e_g + v, \quad (25)$$

where $e_g = x_g - x_{g_\star}$, $x_{g_\star}$ is a desired equilibrium point, v is an additional damping injection, which is selected as

$$v = -R_a e_g \quad (26)$$

with the damping injection matrix given by

$$R_a = \text{diag}\{R_1, R_2, R_3, R_4, R_5\} \succeq 0 \quad (27)$$

[2]See [35] for further details of the input-affine system and S-PBC.

A replication of the system dynamics of SHP (11) is proposed, as follows

$$D_g \dot{x}_{g_\star} = \big(J(x) - R_g(x)\big)\, x_{g_\star} r + b(x) + G u_g + v. \quad (28)$$

Now, subtracting (11) from (28) and employing (26) yields the system described in (29):

$$D_g \dot{e}_g = (J(x) - R_\star)\, e_g, \quad (29)$$

where $R_\star = R_g(x) + R_a > 0$.

The system (25) is asymptotically stable at any equilibrium point with the control law u_g. In order to see this, let us define a Lyapunov function candidate

$$V_g(e_g) = \frac{1}{2} e_g^\top D_g e_g, \quad (30)$$

and, taking its time derivative yields

$$\begin{aligned} \dot{V}_g(e_g) &= e_g^\top D_g \dot{e}_g \\ &= e_g^\top (J_\star - R_\star)\, e_g \\ &= -e_g^\top R_\star e_g < 0, \end{aligned} \quad (31)$$

if $R_\star$ is a positive definite matrix, $\dot{V}_g(e_g) < 0$ is asymptotically stable, which implies that x_g converges asymptotically to $x_{g_\star}$ [30].

1) CONTROLLER DESIGN FOR THE SHP

This section presents the controller design for the SHP based on the previously presented S-PBC theory. The control laws are found from (28), as follows

$$\begin{aligned} u_y &= x_{2\star} - R_2(x_2 - x_{2\star}), \\ m_{dg} &= -\frac{R_3(x_3 - x_{3\star}) + R_g x_{3\star} - L_g x_5 x_{4\star}}{v_{dc}}, \\ m_{qg} &= -\frac{R_4(x_4 - x_{4\star}) + R_g x_{4\star} + L_g x_5 x_{3\star}}{v_{dc}} \\ &\quad + \frac{\psi x_{5\star}}{v_{dc}}. \end{aligned} \quad (32)$$

Now, the reference values for the SHP needs to be defined. Typically, the PMSG's the control variables are rotor speed and direct axis current. $x_{5_\star}$ allows control of the rotor speed, i.e., $x_{5_\star} = \omega_m^{nom}$ and to guarantee the maximum torque $x_{3_\star} = 0$. To control the electrical power delivered by PMSG, we use the following expression

$$x_{2_\star} = \frac{A_t x_{1\star}^2 (x_{1\star} - q_{nl})}{P_{m_\star}}, \quad (33)$$

with,

$$P_{m_\star} = P_{e_\star} + |i_{dq}|^2 R_g, \quad (34)$$

where $P_{e_\star}$ is the reference electrical power, and the admissible trajectories for the non-controlled variables are achieved from (28), which generate:

$$x_{4_\star} = \frac{T_m + R_5(x_5 - x_{5_\star})}{\psi}, \quad (35)$$

$$x_{1_\star} = \frac{R_1 x_1 - 1}{R_1 - x_1 \left(k_f + \dfrac{1}{x_2^2}\right)}. \quad (36)$$

B. PASSIVITY-BASED PI CONTROL

Given that the system (18) is an input-non-affine system, it is sufficient to employ PI-PBC.[3]

Let $x_{v\star}$ define an admissible trajectory of the system (18). I.e., $x_{v\star}$ is an equilibrium trajectory on (18) if it exists, is differentiable, is bounded if it satisfies

$$D\dot{x}_{v_\star} = \left(J_o + \sum_{i=1}^{2} J_i u_{vi_\star} - R_v\right) x_{v_\star} + d_v, \tag{37}$$

and it is produced by some bounded control signals $u_{v_\star}$. An admissible trajectory $x_{v_\star}$ of a dynamical system is just a solution which belongs to the flow of the differential equation for a bounded input $u_{v_\star}$. An admissible trajectory $x_{v_\star}$ is not reached if there is no bounded $u_{v_\star}$ that generates it. The admissible trajectory concept is indispensable for designing controllers based on passivity-based theory.

1) PASSIVE CONTROL FOR pH INCREMENTAL MODELS

This section presents an incremental model of the dynamical system shown in (18) and it is demonstrated that the incremental model is passive.

The dynamical system presented in (38) is defined based on the incremental model, i.e., $e_v = x_v - x_{v_\star}$ and $\tilde{u}_v = u_v - u_{v_\star}$ are substituted into (18).

$$D_v\dot{e}_v = \left(J_o + \sum_{i=1}^{2} J_i(\tilde{u}_i + u_{vi_\star}) - R_v\right)(e_v + x_{v_\star}) + d_v, \tag{38}$$

and for an output function defined as $y_v = C(x_{v_\star})^4 x_v$, where

$$C(x_{v_\star}) = -\begin{bmatrix} x_{v_\star}^\top J_1 \\ x_{v_\star}^\top J_2 \end{bmatrix}, \tag{39}$$

is passive, if it satisfies the dissipation inequality $\dot{S} \leq \tilde{y}_v^\top \tilde{u}_v$, where

$$\tilde{y}_v = C(x_{v_\star})e_v, \tag{40}$$

and the storage function is given by

$$S(e_v) = \frac{1}{2} e_v^\top D e_v. \tag{41}$$

Applying the temporal derivative of the storage function (41) along the trajectories of (38), the following equation is obtained.

$$\begin{aligned}
\dot{S}(e_v) &= e_v^\top D\dot{e}_v \\
&= e_v^\top \left(J_o + \sum_{i=1}^{2} J_i u_{vi} - R_v\right) e_v + e_v^\top \sum_{i=1}^{2} J_i \Delta u_{vi} x_{v_\star} \\
&= -e_v^\top R_v e_v + e_v^\top \sum_{i=1}^{2} J_i \Delta u_{vi} x_{v_\star} \\
&\leq e_v^\top \sum_{i=1}^{2} J_i \Delta u_{vi} x_{v_\star} \\
&= \tilde{y}_v^\top \tilde{u}_v,
\end{aligned} \tag{42}$$

This proves that the system (38) is passive from $u_v \longrightarrow y_v$.

[3]See [36] for further details of the input-non-affine system and PI-PBC.

[4]This matrix was already established in [33].

2) PI GLOBAL TRACKING CONTROLLER

The VSC described by (18) can be controlled in closed-loop by the controller

$$\dot{z} = \tilde{y}_v, \tag{43}$$

$$\tilde{u}_v = -K_p\tilde{y}_v - K_i z, \tag{44}$$

and output y_v by (40). Consider gain matrices in which $K_p = K_p^\top > 0$, $K_i = K_i^\top > 0$, and fulfilling some admissible trajectory $x_{v\star}$ given by (37). To achieve global tracking for any initial conditions $(x_v(0), z_v(0))$ of the system (18), it is necessary to satisfy the rank condition $rank(M) = n$, with

$$y_a = \begin{bmatrix} C(x_{v_\star}) \\ Q^{\frac{1}{2}} \end{bmatrix} e_v = M e_v \tag{45}$$

then,

$$\lim_{t \longrightarrow \infty} x_v = x_{v_\star}. \tag{46}$$

This property was already reported in [33].

Let us define a Lyapunov function candidate as

$$V(e_v) = S(e_v) + \frac{1}{2} z_v^\top K_{i_v} z_v. \tag{47}$$

Calculating the time derivative (47) along (38) gives

$$\dot{V}(e_v) = \dot{S}(e_v) + \frac{1}{2} z_v^\top K_{i_v} \dot{z}_v \tag{48}$$

$$= -e_v^\top R_v e_v - y_v^\top K_{p_v} y_v \tag{49}$$

3) CONTROLLER DESIGN OF THE VSC

This section presents the controller design of the VSC based on PI-passive theory shown above. Applying (40), the passive outputs are

$$\tilde{y}_v = \begin{bmatrix} x_8 x_{6_\star} - x_6 x_{8_\star} \\ x_8 x_{7_\star} - x_7 x_{8_\star} \end{bmatrix}, \tag{50}$$

and, the asymptotic convergence condition is checked by means of the following matrix

$$M = \begin{bmatrix} x_{8_\star} & 0 & -x_{6_\star} \\ 0 & x_{8_\star} & -x_{7_\star} \\ \sqrt{R} & 0 & 0 \\ 0 & \sqrt{R} & 0 \\ 0 & 0 & 0 \end{bmatrix}, \tag{51}$$

while $x_{6_\star}$ or $x_{7_\star}$ are bounded away from zero, the full-rank condition is fulfilled and x_v will converge to $x_{v\star}$ asymptotically. This situation occurs in normal operation of the VSC since PMSG is always generating the active power, i.e., $x_{6_\star} > 0$.

Defining x_8 and x_7 as the reference values for the VSC. $x_{8_\star}$ is selected to control dc-link voltage on the capacitor C, i.e., $x_{8_\star} = V_{dc}^{nom}$. The $x_{7_\star}$ permits us to control the reactive power delivered (or absorbed) by VSC to the ac grid, which is calculated as

$$x_{7_\star} = \frac{e_q P_{e\star} - e_q Q_\star}{e_d^2 + e_q^2}, \tag{52}$$

where $Q_\star$ is the reference reactive power and $P_{e\star}$ is the active power delivered by PMSG.

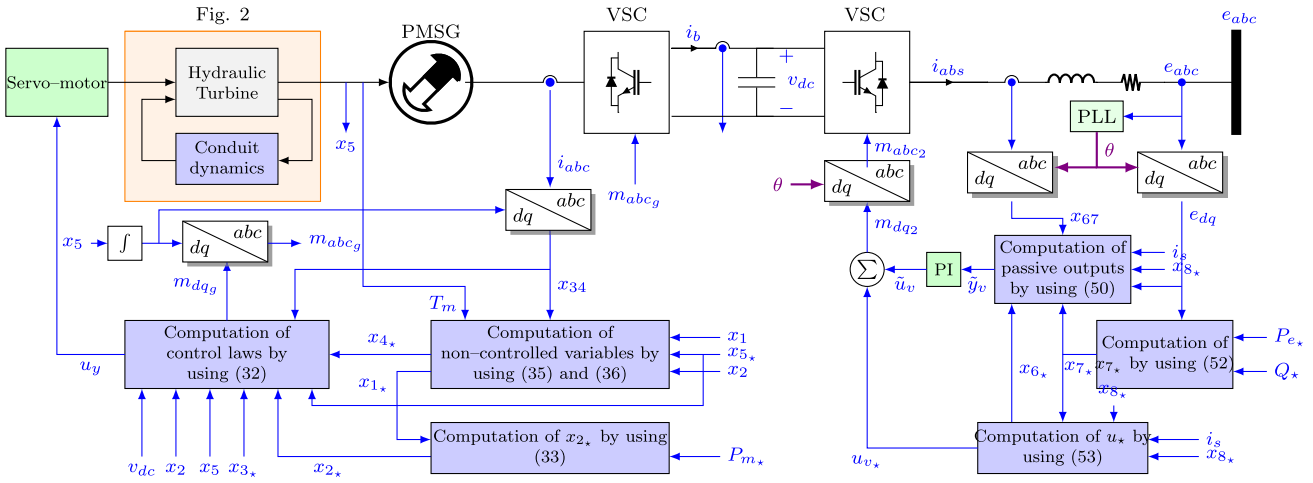

FIGURE 3. Control scheme of the proposed controllers applied to small hydro-power plant.

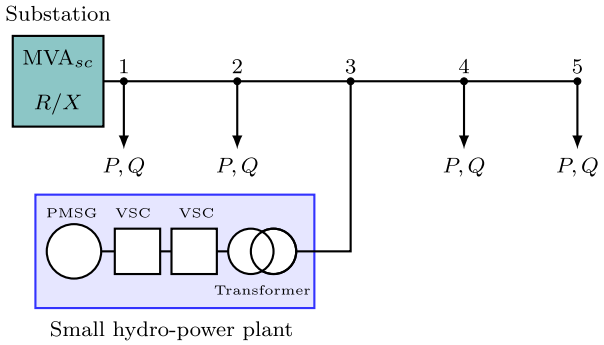

FIGURE 4. Simulated primary feeder with a small hydro-power plant.

The controller design is fulfilled when $x_{6_\star}$, $m^\star_{d2}$ and $m^\star_{q2}$ are determined. Therefore, the admissible trajectory for VSC is achieved from (37), and given by

$$m^\star_{d2} = \frac{L\dot{x}_{6_\star} + L\omega x_{7_\star} + e_d + Rx_{6_\star}}{x_{8_\star}},$$
$$m^\star_{q2} = \frac{L\dot{x}_{7_\star} - L\omega x_{6_\star} + e_q + Rx_{7_\star}}{x_{8_\star}},$$
$$x_{6_\star} = \frac{-C\dot{x}_{8_\star} + i_s - m^\star_{q2}x_{7_\star}}{m^\star_{d2}}. \quad (53)$$

Fig. 3 illustrates the control scheme of the proposed controllers.

IV. SIMULATIONS AND RESULTS

A. THE STUDIED SYSTEM

Fig. 4 depicts the test system employed to assess the proposed controller. This test system is a modification of the one introduced in [28], which has a 13.2 kV distribution feeder with a 2-MW SHP and four loads. The parameters of the system and SHP are listed in Table 1.

B. SIMULATION CASES

We propose three simulation cases in order to investigate the effectiveness of the proposed controller of the SHP, and the simulations were implemented using MATLAB/Simulink.

TABLE 1. Parameters of the system.

Parameter	Value	Unit	Component
Nominal power	2	MVA	PMSG
Nominal voltage	690	V	
Nominal rotational speed	$2\pi 34$	rad/s	
Stator phase resistance	0.05	pu	
Armature impedance	0.80	pu	
Flux	1.50	pu	
Starting time of water in tunnel	4	s	SHP
Factor of constant proportionality	1.65		
Servomotor main time constant	0.3	s	
Friction losses on penstock	$1.7 \cdot 10^{-4}$	pu	
Nominal voltage	13.2	kV	Grid
Three-phase short circuit power	100	MW	
X/R ratio	7		
Frequency	60	Hz	
Nominal power	2	MVA	VSC
Inductor L	1.2669	pu	
Resistor R	0.21	pu	
Capacitor C	1.375	pu	
Nominal dc voltage	1200	V	

For validation, the proposed controller is compared with a conventional PI controller. It is important to note that when we refer to the PI controller for the SHP, it is divided as follows: the governor system is controlled with the PID controller, while the PMSG and the VSC are controlled with PI controllers.

The parameters of the proposed controllers and PI controller are listed in Table 2.

1) CASE I

In this case, it presents the ability of the PBC to control the active and reactive output power of the SHP on the point of common coupling (PCC).

The simulation results illustrated in Fig. 5 show the active power delivered by the hydro-power plant on the dc-link and the rotor speed deviation.

Note in Fig. 5(a) that the response of both controllers presents the intrinsic non-minimum phase characteristic of the hydro-power plant. However, the PBC has a better response than the PI controller with an average error of

TABLE 2. Proposed controllers and PI controller parameters.

Parameter	Value	Unit	Controller
Damping gain R_1	1	pu	S-PBC
Damping gain R_2	100	pu	
Damping gain R_3	25	pu	
Damping gain R_4	5	pu	
Damping gain R_5	1000	pu	
Proportional gain K_p	2	pu	PI-PBC
Integral gain K_i	0.1	pu	
Proportional gain K_p	1.1072	pu	PID speed governor
Integral gain K_i	0.0831	pu	
Derivative gain K_d	2.2144	pu	
Proportional gain K_p for i_d	30	pu	PI PSMG Control
Integral gain K_i for i_d	100	pu	
Proportional gain K_p for i_q	50	pu	
Integral gain K_i for i_q	300	pu	
Proportional gain K_p	2	pu	Outer Control
Integral gain K_i	0.1	pu	
Proportional gain K_p	25	pu	Inner Control
Integral gain K_i	1.5	pu	

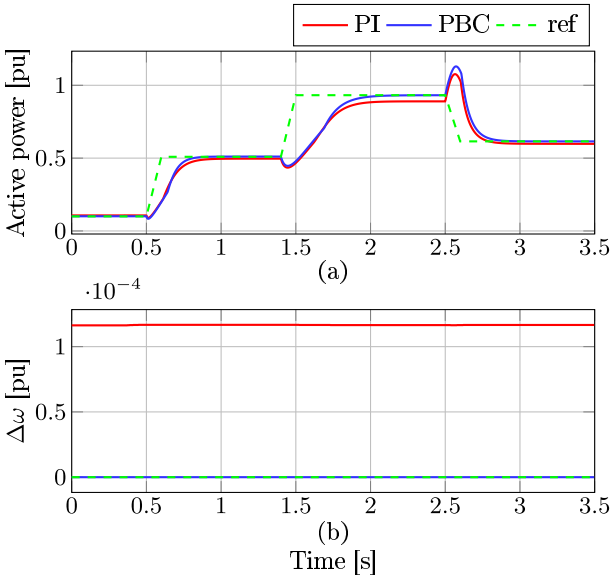

FIGURE 5. Dynamic response of PMSG for Case I. (a) active power generated by PMSG on dc-link, and (b) rotor speed deviation.

around 5%, while the PI controller presents an average error of around 8.4%. For rotor speed regulation, the proposed controller continues to show a better performance than the PI controller since this maintains an error of around $1 \cdot 10^{-4}$ (see Fig. 5(b)).

Fig. 6 shows the active and reactive power delivered on PCC by the SHP and the dc-link voltage. By comparing Fig. 6(a) with Fig. 5(a), it is observed that the active power behavior is maintained where the PBC presents an average error of around 6.4%, while the PI controller has an average error of around 9.2%.

Observe in Fig. 6(b) that both controllers follow the desired reference. However, the proposed controller shows a better dynamic response than the PI controller with a standard deviation of 0.6%, while the PI controller has a standard deviation of 0.9%. For the voltage regulation, both controllers present similar behavior.

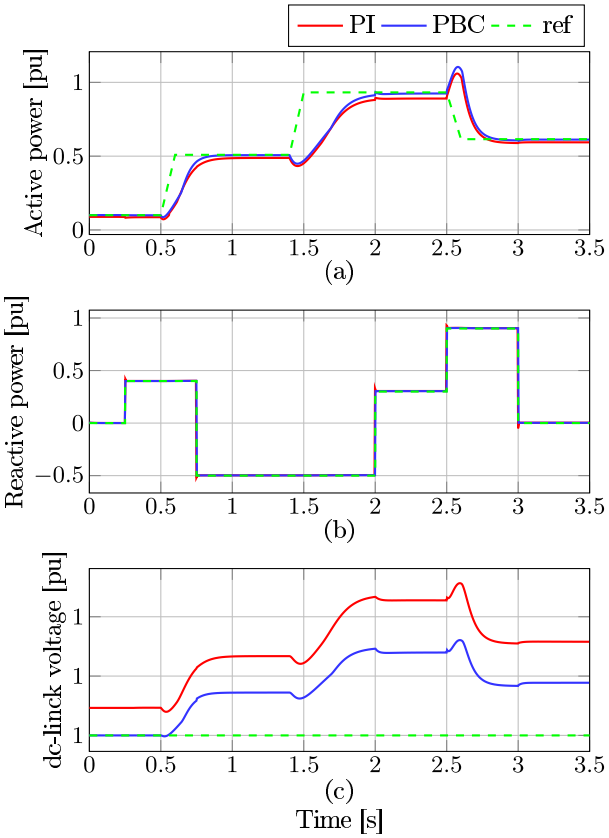

FIGURE 6. Dynamic response of the SHP on PCC for Case I. (a) Active power delivered, (b) Reactive power generated, and (c) voltage on capacitor.

2) CASE II

This case investigates the performance of the proposed controller when the SHP system delivers from low to high power. The active power reference starts at 0.1 pu and in $t = 0.4$ s the reference changes to 0.93 pu. The results are illustrated in Figs. 7 and 8. The active power provided by the PMSG for both controllers is depicted in Fig. 7(a). Note that the proposed controller continues to show a better response than the PI controller. The proposed controller has an average error of around 22.5%, while the PI controller has an average error of around 25.4%. It is important to mention that average errors are high since the settling time is approximately 0.7 s.

Observe in Fig. 7(b) that rotor speed deviation has the same behavior as shown in case I (see Fig. 6(b)). Hence, the PBC continues to demonstrate better performance than the PI controller since the conventional controller maintains an error of around $1.16 \cdot 10^{-4}$.

Analyzing Figs. 7(a) and 8(a), it can be observed that the active power behavior is maintained when the PBC and the PI controllers are implemented and the average errors are around 24.4% and 28.6%, respectively.

Note that in Fig. 8(b), both controllers can follow the desired reference. However, the PBC has a better dynamic response than the PI controller with a standard deviation of 1.1%, while the PI controller has a standard deviation

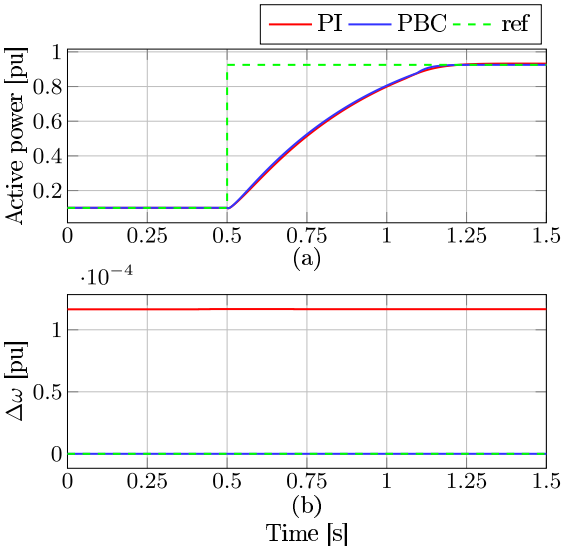

FIGURE 7. Dynamic response of PMSG for Case II: (a) Active power generated by PMSG on dc-link, and (b) Rotor speed deviation.

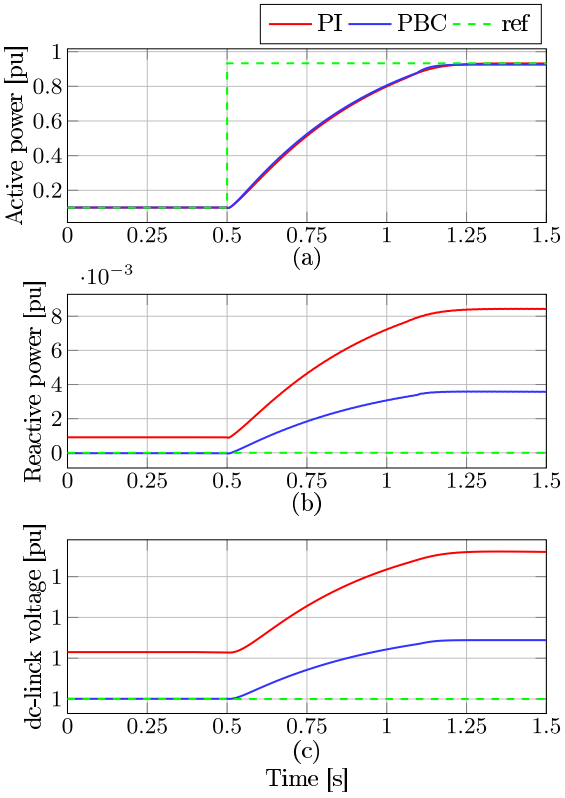

FIGURE 8. Dynamic response of the SHP on PCC for Case II. (a) Active power delivered, (b) Reactive power generated, and (c) Voltage on capacitor.

of 1.7%. For the voltage regulation, both controllers present similar behavior.

3) CASE III

The transient behavior of the SHP is analyzed in this case. The active power generated by the SHP is maintained constant at 0.9 pu. A three-phase short-circuit to ground at node-3

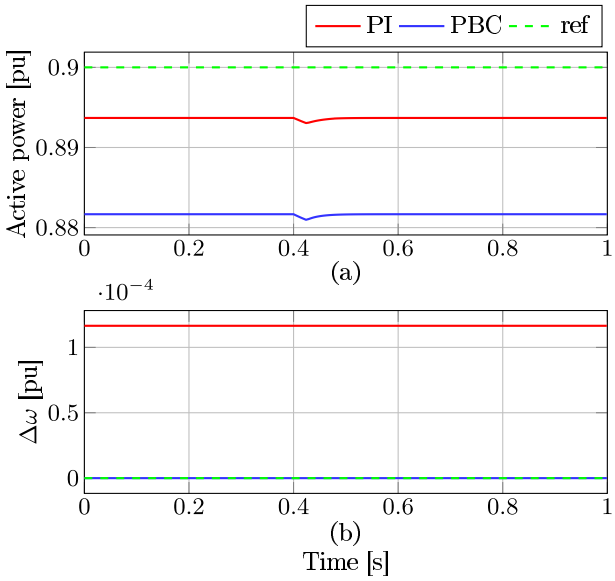

FIGURE 9. Dynamic response of PMSG for Case III: (a) Active power generated by PMSG on dc-link, and (b) Rotor speed deviation.

is considered in $t = 0.4$ s. The results are presented in Figs. 9 and 10. The active power generated for both controllers on the dc-link voltage decreases due to the grid voltage drop at Node-3. However, both controllers returned to initial values (see Fig. 9(a)). The rotor speed maintains its speed during the fault (see Fig. 9(b)).

The active power delivered on PCC decreases to almost zero for both controllers. Next, when the fault is removed, the active power provided by the PBC has a higher peak than the PI controller. However, the proposed controller stabilizes the system in less time compared with the PI controller (see Fig. 10(a)). Note in Fig. 10(b) and 10(c) that both controllers show the same dynamic response for the reactive power and dc-link voltage, respectively.

4) COMPLEMENTARY ANALYSIS

To quantify the performance of the proposed controller, the integral of the time-weighted absolute error (Δ) is used. The settling time t_p for the active power delivered by the PMSG is also considered. Δ-values are computed for the rotor speed deviation, the dc-link voltage, the active power delivered by the PMSG, and the reactive power, as follows

$$\begin{aligned}
\Delta_{\omega} &= \int_0^{t_{sim}} t' \left|\omega - 1\right| dt', \\
\Delta_{v_{dc}} &= \int_0^{t_{sim}} t' \left|v_{dc} - v_{dc}^{\star}\right| dt', \\
\Delta_{p} &= \int_0^{t_{sim}} t' \left|P_e - P_e^{\star}\right| dt', \\
\Delta_{q} &= \int_0^{t_{sim}} t' \left|Q - Q^{\star}\right| dt'
\end{aligned} \tag{54}$$

where t_{sim} is the simulation time.

Table 3 shows the performance indices for each case considered. Note that these indices validate the enhanced performance for the proposed controller from the perspective

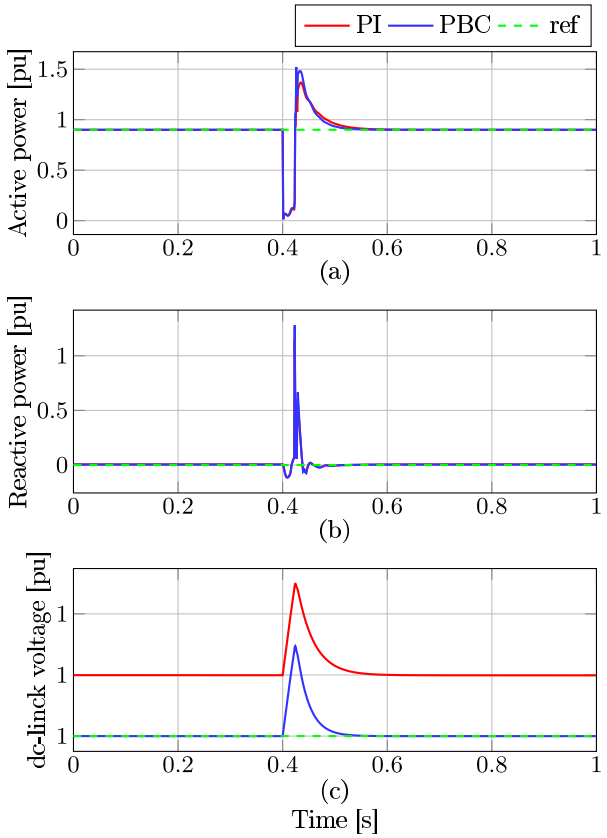

FIGURE 10. Dynamic response of the SHP on PCC for Case III. (a) Active power delivered, (b) Reactive power generated, and (c) Voltage on capacitor.

TABLE 3. Performance indices.

	Control	Δ_ω	$\Delta_{v_{dc}}$	Δ_p	Δ_q	t_p [s]
Case I	PI	0.204	0.610	123.76	26.824	0.354
	PBC	5^{-7}	0.351	105.363	10.142	0.322
Case 2	PI	0.058	0.264	16.371	4.754	0.14
	PBC	4.5^{-8}	0.012	1.040	5.440	0.111
Case 3	PI	0.263	1.293	310.805	16.374	0.85
	PBC	3.5^{-7}	0.463	300.401	5.819	0.711

of less steady-state error and reduced settling time of each case proposed.

V. CONCLUSION

A new approach for the control of SHPs based on passivity theory was described in this paper. The SHP consisted of a PMSG connected to a three-phase grid through a back-to-back converter. The S-PBC and PI-PBC approaches for an SHP connected to a test feeder system were described. These controllers guarantee asymptotic stability through Lyapunov's theory. The controllers were assessed and compared with the classic PI controller considering state and transients behaviors in SHPs. It was observed that the controllers based on PBC showed better performance in all cases considered compared to the PI controllers. This has been confirmed by comparing with the integral of time-weighted absolute error and settling time.

REFERENCES

[1] W. J. Gil-Gonzalez, A. Garces, O. B. Fosso, and A. Escobar-Mejia, "Passivity-based control of power systems considering hydro-turbine with surge tank," *IEEE Trans. Power Syst.*, vol. 35, no. 3, pp. 2002–2011, May 2020.
[2] C. Xu and D. Qian, "Governor design for a hydropower plant with an upstream surge tank by GA-based fuzzy reduced-order sliding mode," *Energies*, vol. 8, no. 12, pp. 13442–13457, Nov. 2015.
[3] D. Borkowski, "Analytical model of small hydropower plant working at variable speed," *IEEE Trans. Energy Convers.*, vol. 33, no. 4, pp. 1886–1894, Dec. 2018.
[4] P. Hušek, "PID controller design for hydraulic turbine based on sensitivity margin specifications," *Int. J. Electr. Power Energy Syst.*, vol. 55, pp. 460–466, Feb. 2014.
[5] X. Yu, J. Zhang, C. Fan, and S. Chen, "Stability analysis of governor-turbine-hydraulic system by state space method and graph theory," *Energy*, vol. 114, pp. 613–622, Nov. 2016.
[6] H. Fang, L. Chen, and Z. Shen, "Application of an improved PSO algorithm to optimal tuning of PID gains for water turbine governor," *Energy Convers. Manage.*, vol. 52, no. 4, pp. 1763–1770, Apr. 2011.
[7] M. Beus and H. Pandžić, "Application of an adaptive model predictive control algorithm on the Pelton turbine governor control," *IET Renew. Power Gener.*, vol. 14, no. 10, pp. 1720–1727, 2020.
[8] X. Gong, "Optimization of the power generation control process of hydraulic turbine set based on the improved BFO-PSO algorithm," *J. Coastal Res.*, vol. 94, no. sp1, p. 227, Sep. 2019.
[9] W. Guo, J. Yang, M. Wang, and X. Lai, "Nonlinear modeling and stability analysis of hydro-turbine governing system with sloping ceiling tail-race tunnel under load disturbance," *Energy Convers. Manage.*, vol. 106, pp. 127–138, Dec. 2015.
[10] D. Chen, C. Ding, Y. Do, X. Ma, H. Zhao, and Y. Wang, "Nonlinear dynamic analysis for a francis hydro-turbine governing system and its control," *J. Franklin Inst.*, vol. 351, no. 9, pp. 4596–4618, Sep. 2014, doi: 10.1016/j.jfranklin.2014.07.002.
[11] X. Yuan, Z. Chen, Y. Yuan, Y. Huang, X. Li, and W. Li, "Sliding mode controller of hydraulic generator regulating system based on the input/output feedback linearization method," *Math. Comput. Simul.*, vol. 119, pp. 18–34, Jan. 2016.
[12] O. Cerman and P. Hušek, "Adaptive fuzzy sliding mode control for electro-hydraulic servo mechanism," *Expert Syst. Appl.*, vol. 39, no. 11, pp. 10269–10277, Sep. 2012, doi: 10.1016/j.eswa.2012.02.172.
[13] K. Nagode and I. Škrjanc, "Modelling and internal fuzzy model power control of a francis water turbine," *Energies*, vol. 7, no. 2, pp. 874–889, Feb. 2014.
[14] C. Li, Y. Mao, J. Zhou, N. Zhang, and X. An, "Design of a fuzzy-PID controller for a nonlinear hydraulic turbine governing system by using a novel gravitational search algorithm based on cauchy mutation and mass weighting," *Appl. Soft Comput.*, vol. 52, pp. 290–305, Mar. 2017.
[15] S. Simani, S. Alvisi, and M. Venturini, "Fault tolerant control of a simulated hydroelectric system," *Control Eng. Pract.*, vol. 51, pp. 13–25, Jun. 2016.
[16] R. Zhang, D. Chen, and X. Ma, "Nonlinear predictive control of a hydropower system model," *Entropy*, vol. 17, no. 9, pp. 6129–6149, 2015.
[17] W. Zhu, Y. Zheng, J. Dai, and J. Zhou, "Design of integrated synergetic controller for the excitation and governing system of hydraulic generator unit," *Eng. Appl. Artif. Intell.*, vol. 58, pp. 79–87, Feb. 2017.
[18] C. Ma, C. Liu, X. Zhang, Y. Sun, W. Wu, and J. Xie, "Fixed-time stability of the hydraulic turbine governing system," *Math. Problems Eng.*, vol. 2018, pp. 1–10, Jan. 2018.
[19] D. Borkowski and T. Wegiel, "Small hydropower plant with integrated turbine-generators working at variable speed," *IEEE Trans. Energy Convers.*, vol. 28, no. 2, pp. 452–459, Jun. 2013.
[20] D. Borkowski, "Average-value model of energy conversion system consisting of PMSG, diode bridge rectifier and DPC-SVM controlled inverter," in *Proc. Int. Symp. Electr. Mach. (SME)*, Jun. 2017, pp. 1–6.
[21] N. Hamouda, H. Benalla, K. Hemsas, B. Babes, J. Petzoldt, T. Ellinger, and C. Hamouda, "Type-2 fuzzy logic predictive control of a grid connected wind power systems with integrated active power filter capabilities," *J. Power Electron.*, vol. 17, no. 6, pp. 1587–1599, 2017, doi: 10.6113/JPE.2017.17.6.1587.
[22] A. Beddar, H. Bouzekri, K. Hemsas, B. Babes, and H. Afghoul, "Real time implementation of improved fractional order proportional-integral controller for grid connected wind energy conversion system," *Rev. Roum. Sci. Tech. Ser. électrotech. énerg*, vol. 61, no. 4, pp. 402–407, 2016.

[23] J. L. Márquez, M. G. Molina, and J. M. Pacas, "Dynamic modeling, simulation and control design of an advanced micro-hydro power plant for distributed generation applications," *Int. J. Hydrogen Energy*, vol. 35, no. 11, pp. 5772–5777, Jun. 2010.
[24] D. Ling and Y. Tao, "An analysis of the hopf bifurcation in a hydroturbine governing system with saturation," *IEEE Trans. Energy Convers.*, vol. 21, no. 2, pp. 512–515, Jun. 2006, doi: 10.1109/TEC.2005.860407.
[25] B. Babes, L. Rahmani, A. Chaoui, and N. Hamouda, "Design and experimental validation of a digital predictive controller for variable-speed wind turbine systems," *J. Power Electron.*, vol. 17, no. 1, pp. 232–241, Jan. 2017, doi: 10.6113/JPE.2017.17.1.232.
[26] J. Machowski, Z. Lubosny, J. Bialek, J. Bumby, *Power System Dynamics: Stability and Control*, 3rd ed. Hoboken, NJ, USA: Wiley, 2020.
[27] J. A. Baroudi, V. Dinavahi, and A. M. Knight, "A review of power converter topologies for wind generators," *Renew. Energy*, vol. 32, no. 14, pp. 2369–2385, Nov. 2007.
[28] E. Giraldo and A. Garces, "An adaptive control strategy for a wind energy conversion system based on PWM-CSC and PMSG," *IEEE Trans. Power Syst.*, vol. 29, no. 3, pp. 1446–1453, May 2014.
[29] S. Golestan, J. M. Guerrero, and J. C. Vasquez, "Three-phase PLLs: A review of recent advances," *IEEE Trans. Power Electron.*, vol. 32, no. 3, pp. 1894–1907, Mar. 2017.
[30] A. van der Schaft, *L2-Gain and Passivity Techniques in Nonlinear Control*, 3rd ed. London, U.K.: Springer, 2017.
[31] T. Xu, L. Zhang, Y. Zeng, and J. Qian, "Hamiltonian model of hydro turbine with sharing common conduit," in *Proc. Asia–Pacific Power Energy Eng. Conf.*, Mar. 2012, pp. 1–5, doi: 10.1109/APPEEC.2012.6307009.
[32] R. Ortega, A. van der Schaft, B. Maschke, and G. Escobar, "Interconnection and damping assignment passivity-based control of port-controlled Hamiltonian systems," *Automatica*, vol. 38, no. 4, pp. 585–596, 2002, doi: 10.1016/S0005-1098(01)00278-3.
[33] R. Cisneros, M. Pirro, G. Bergna, R. Ortega, G. Ippoliti, and M. Molinas, "Global tracking passivity-based PI control of bilinear systems: Application to the interleaved boost and modular multilevel converters," *Control Eng. Pract.*, vol. 43, pp. 109–119, Oct. 2015.
[34] F. Mancilla-David and R. Ortega, "Adaptive passivity-based control for maximum power extraction of stand-alone windmill systems," *Control Eng. Pract.*, vol. 20, no. 2, pp. 173–181, Feb. 2012.
[35] R. Ortega, J. A. L. Perez, P. J. Nicklasson, and H. J. Sira-Ramirez, *Passivity-Based Control of Euler-Lagrange Systems: Mechanical, Electrical and Electro-Mechanical Applications*. Berlin, Germany: Springer, 2013.
[36] R. C. Montoya, "PI passivity-based control: Application to physical systems," Ph.D. dissertation, Dept. Autom., Univ. Paris-Saclay, Essonne, France, 2016.

WALTER GIL-GONZÁLEZ (Member, IEEE) was born in Pereira, Colombia, in 1986. He received the B.Sc., M.Sc., and Ph.D. degrees in electrical engineering from the Universidad Tecnológica de Pereira, Colombia, in 2011, 2013, and 2019, respectively. He is currently working as an Adjunct Professor with the Department of Electric Power Engineering, Institución Universitaria Pascual Bravo. His research interests include power systems' control and stability and optimization and operation of the power systems.

ALEJANDRO GARCÉS (Senior Member, IEEE) was born in Pereira, Colombia, in 1981. He received the bachelor's degree in electrical engineering and the master's degree in power systems engineering from the Universidad Tecnológica de Pereira, Pereira, in 2004 and 2006, respectively, and the Ph.D. degree from the Norwegian University of Science and Technology (NTNU), Trondheim, Norway, in 2012. He was a Research Fellow with NTNU. He was also a Consultant with the Inter-American Development Bank, the Latin-American Organization of Energy, and the Energy and Gas Regulation Commission, Colombia. He has participated with the study Smart Grids Colombia Vision 2030 that defined the roadmap for the implementation of smart grids in Colombia. He is currently an Assistant Professor with the Department of Electric Power Engineering, Universidad Tecnológica de Pereira. His current research interests include mathematical optimization and control for power systems applications, dynamics in electric grids, renewable energies, energy storage devices, microgrids, and HVDC transmission.

OLAV B. FOSSO (Senior Member, IEEE) was a Scientific Advisor and a Senior Research Scientist with the Head of the Department of Electric Power Engineering, SINTEF Energy Research, from 2009 to 2013. He was also the Director of the Norwegian University of Science and Technology (NTNU) Strategic Thematic Area Energy from 2014 to 2016. He is currently a Professor with the Department of Electric Power Engineering, NTNU, Trondheim, Norway. His research interests include hydro scheduling, market integration of intermittent generation, and signal analysis for the study of power systems dynamics and stability. He was a member of the CIGRE Technical Committee from 2008 to 2014 and a Board Member of the Norwegian National Strategy Energy21 from 2015 to 2018. He was the Chairman of the CIGRE SC C5 Electricity Markets and Regulation and the Board of NOWITECH from 2015 to 2017.